Metal Tungstates at the Ultimate Two-Dimensional Limit: Fabrication of a $CuWO_4$ Nanophase

Martin Denk,[†] David Kuhness,[†] Margareta Wagner,[†] Svetlozar Surnev,[†] Fabio R. Negreiros,[‡] Luca Sementa,[‡] Giovanni Barcaro,[‡] Ivana Vobornik,[§] Alessandro Fortunelli,[‡] and Falko P. Netzer[†,*]

[†]Surface and Interface Physics, Institute of Physics, Karl-Franzens University A-8010 Graz, Austria, [‡]CNR-ICCOM and IPCF, Consiglio Nazionale delle Ricerche, via G. Moruzzi 1, I-56124 Pisa, Italy, and [§]CNR-IOM, TASC Laboratory, AREA Science Park Basovizza, 34149 Trieste, Italy

ABSTRACT Metal tungstates (with general formula MWO_4) are functional materials with a high potential for a diverse set of applications ranging from low-dimensional magnetism to chemical sensing and photoelectrocatalytic water oxidation. For high level applications, nanoscale control of film growth is necessary, as well as a deeper understanding and characterization of materials properties at reduced dimensionality. We succeeded in fabricating and characterizing a two-dimensional (2-D) copper tungstate ($CuWO_4$). For the first time, the atomic structure of an ultrathin ternary oxide is fully unveiled. It corresponds to a $CuWO_4$ monolayer arranged in three sublayers with stacking O—W—O/Cu from the interface. The resulting bidimensional structure forms a robust framework with localized regions of anisotropic flexibility. Electronically it displays a reduced band gap and increased density of states close to the Fermi level with respect to the bulk compound. These unique features open a way for new applications in the field of photo- and electrocatalysis, while the proposed synthesis method represents a radically new and general approach toward the fabrication of 2-D ternary oxides.

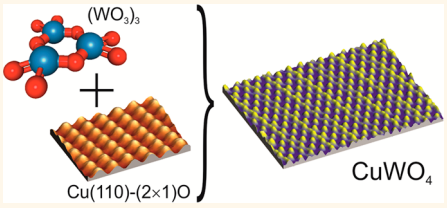

KEYWORDS: two-dimensional oxide material · ternary oxide · Cu tungstate · tungsten oxide clusters · scanning tunneling microscopy · photoelectron spectroscopy · phonon spectra · density functional theory

Ternary tungsten oxides, such as metal tungstates (with general formula MWO_4), are a class of functional materials with fascinating properties at the cutting edge of fundamental science as well as with a high potential for a diverse set of applications in optics, optoelectronics, low-dimensional magnetism, photochemistry, and photocatalysis.[1−13] For example, Cu tungstate ($CuWO_4$), the title compound of this work, displays low-dimensional antiferromagnetic behavior,[6] is commonly used as chemical sensor and scintillating material, and has been advocated as a promising photoanode for photoelectrocatalytic water oxidation due to its band gap of 2.25 eV and excellent visible-light harvesting capability.[8,12] However, for high level applications, in view of shrinking dimensions in nanotechnology, thin film processing with nanoscale control of the active materials going beyond traditional fabrication techniques such as reactive magnetron sputtering and electrochemical deposition[1,8,9] becomes necessary, as well as a deeper understanding and characterization of materials properties. To address these issues, here we report the fabrication of a two-dimensional (2-D) Cu tungstate surface oxide with atomic control using the novel approach of a 2-D solid state chemical reaction, and its structural and spectroscopic complete characterization. The thereby created model system is a suitable platform for a detailed fundamental microscopic understanding of the structure—property relationship in complex low-dimensional oxide systems *via* a close coupling of experimental behavior and first-principles theoretical modeling,[14] and it is further shown to exhibit peculiar structural and electronic properties which make it appealing for photo- and electrocatalytic applications. The method is illustrated for a 2-D $CuWO_4$ monolayer supported on Cu(110), but the approach is general and widely applicable to low-D transition metal tungstate systems.[15]

RESULTS AND DISCUSSION

Figure 1 shows a schematic of the preparation procedure. A single crystalline Cu(110)

* Address correspondence to falko.netzer@uni-graz.at.

Received for review February 12, 2014 and accepted March 11, 2014.

Published online March 11, 2014
10.1021/nn500867y

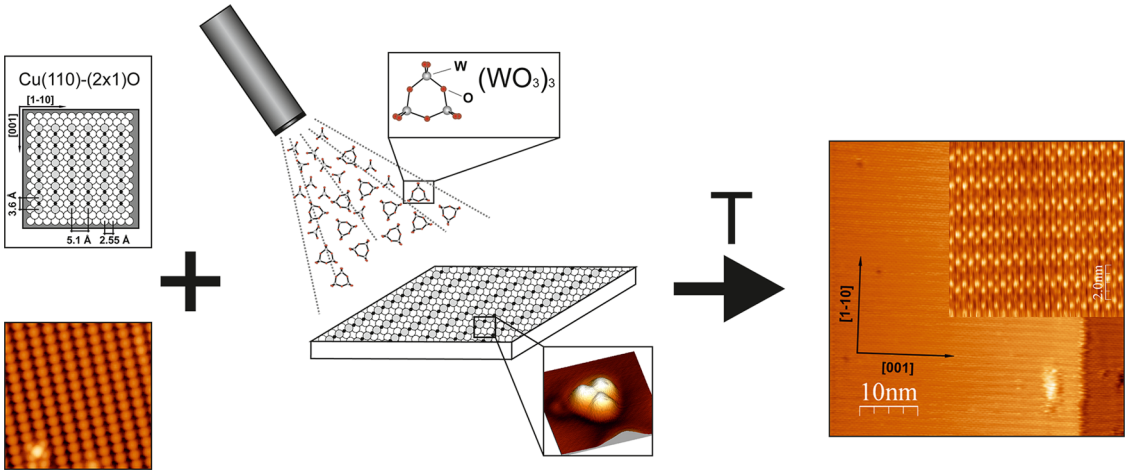

Figure 1. Schematics of the preparation. A single crystalline Cu(110)-(2 × 1)O surface oxide (left) is covered with a monolayer of $(WO_3)_3$ cluster molecules deposited from the gas phase. At low temperature (<100 K), single $(WO_3)_3$ slightly distorted triangular clusters are stable on the surface (middle), whereas at one monolayer coverage and by increasing the surface temperature to T = 600 K, a morphologically flat well ordered oxide overlayer is obtained (right).

surface oxide, prepared *in situ* under ultrahigh vacuum conditions and displaying a well-characterized (2 × 1) surface reconstruction[16] (Figure 1, left), is covered with a monolayer of $(WO_3)_3$ cluster molecules deposited from the gas phase in a monodisperse cluster beam.[17] At low temperature (<100 K), single $(WO_3)_3$ clusters adsorb as stable entities on the Cu-(2 × 1)O surface, displaying a slightly distorted triangular shape in the scanning tunneling microscope (STM) image[18] (Figure 1, middle). At one monolayer coverage and by increasing the surface temperature to 600 K, a surface chemical reaction is initiated: the $(WO_3)_3$ clusters react with the Cu−O surface oxide and create a morphologically flat, well ordered overlayer as illustrated in the STM images of Figure 1, right. As discussed below, this 2-D phase corresponds to a strict monolayer of a Cu−W−O tungstate surface phase, with $CuWO_4$ stoichiometry. It is noted parenthetically that this procedure is loosely related to the traditional fabrication process of metal tungstates in inorganic chemistry, consisting of mixing the respective binary oxide powders followed by high temperature solid state chemical reaction,[19] albeit it is executed here in a low dimensional system under controlled ultrahigh vacuum conditions with atomic precision. In the following, we present the structural, spectroscopic, and theoretical characterization of this Cu−W−O tungstate nanophase and draw a correlation between its structural features and unusual properties.

Structural characterization of the Cu−W−O/Cu(110) layer is provided in Figures 2 and 3. Figure 2(a) shows a low-energy electron diffraction (LEED) pattern, and Figure 2(b) shows STM images with atomic resolution of a surface covered with less than a full oxide monolayer, so that bare Cu-(2 × 1)O areas are coexistent with oxide islands (see upper left part of Figure 2(b)), thus providing an internal calibration. The LEED pattern is complex with sharp diffraction spots, indicative of a well-ordered surface, and several structure elements can be identified: the (2 × 1) unit cell of the Cu−O substrate (white rectangle), a quasisquare unit cell of the Cu−W−O overlayer (indicated in blue), and additional overlayer reflections running in a zigzag line along (0,1) directions (indicated by circles along the dotted line). These structure elements can also be recognized in the Fast Fourier Transform (FFT) of the STM image of Figure 2(b), shown in Figure 2(c). The STM image in Figure 2(b) displays a complicated pattern of atomic-size protrusions with a superimposed contrast modulation of weaker stripes along the [001] direction. An STM line scan across a Cu−W−O oxide island phase boundary to the Cu-(2 × 1)O surface in [1$\underline{1}$0] direction is shown in Figure 2(d): the apparent height of the oxide island is ∼1.1 Å. This is not the true geometric height due to electronic effects in STM imaging,[20] but it is only compatible with a strictly monolayer oxide phase. By combining LEED, STM and FFT data, as discussed in detail in the Supporting Information (SI, see Figure S1), the Cu−W−O oxide layer is derived to possess a rhombic ("quasisquare") unit cell with unit cell vectors **a** ≈ 4.8 Å and an obtuse angle of ∼97° in between them; the stripe contrast modulation superimposed on the quasisquare lattice is a Moiré-type interference effect. Though strictly incommensurate to the Cu(110) substrate, the diagonal of the rhombic unit cell is very closely aligned to the [001] surface direction, which together with a small distortion of lattice vector lengths and angles allows us to approximate this system by a simpler (5 × 2) overlayer-substrate superlattice, very convenient in the following theoretical simulations.

Further information on structural and electronic properties of the Cu−W−O 2-D phase can be obtained from photoelectron spectra and near-edge X-ray

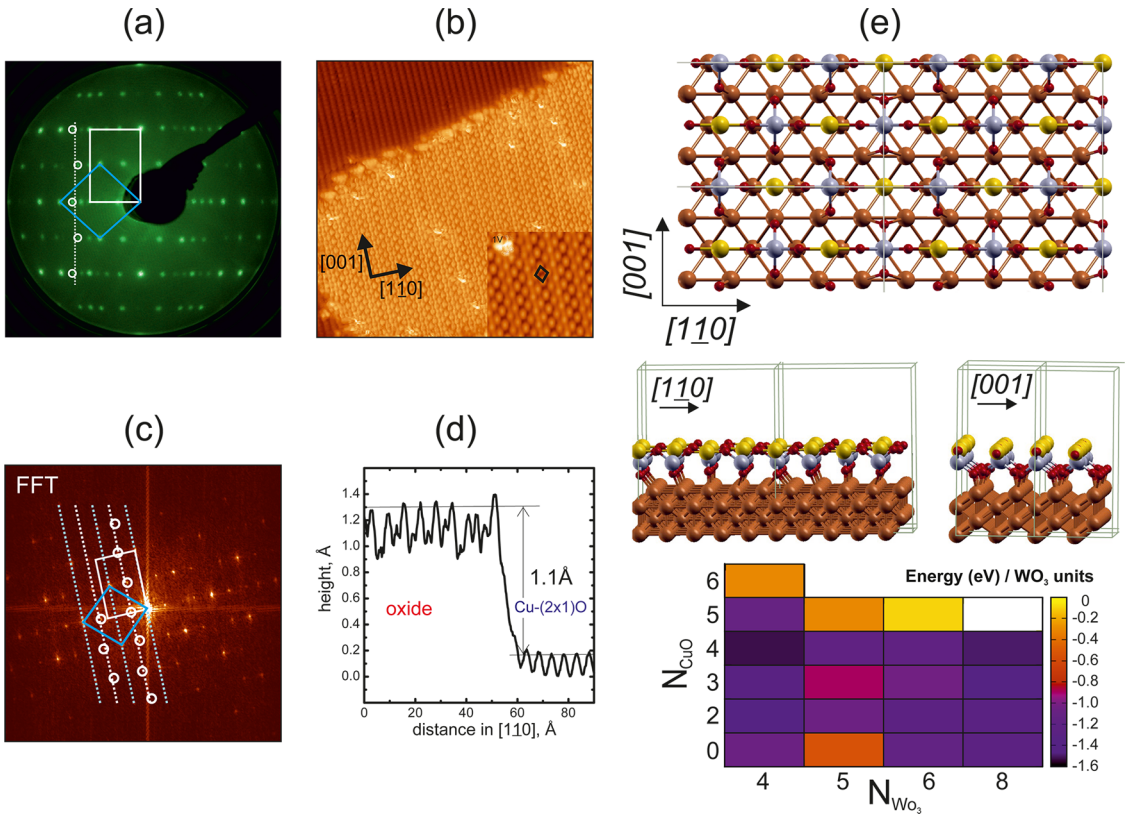

Figure 2. Structure determination. (a) Low-energy electron diffraction (LEED) pattern of the Cu−W−O/Cu(110) layer (electron energy = 82 eV). Several structure elements are indicated; see text. (b) STM images with atomic resolution of a surface covered with less than a full oxide monolayer (200 Å × 200 Å; sample bias V_S = 0.01 V; tunneling current I_T = 0.1 nA; inset: 50 Å × 50 Å; V_S = 1 V, I_T = 0.1 nA). Note the Cu-(2 × 1)O substrate surface at the upper left. (c) Fast Fourier Transform (FFT) of the STM image of panel (b); structure elements as in (a) can be recognized. (d) STM line scan across a Cu−W−O oxide island phase boundary to the Cu-(2 × 1)O surface in [1−10] direction. (e) Top and middle panels: two views of the DFT-derived lowest-energy structure of the $CuWO_4$ 2-D phase corresponding to (N_{WO3}, N_{CuO}) = (4,4) (brown: Cu substrate, red: O, gray: W, yellow: Cu in top surface layer). Bottom panel: ΔE_1 values from eq 1 as a function of N_{WO3} and N_{CuO} are displayed in form of a color plot.

absorption fine structure (NEXAFS) measurements. Figure 3(a−c) displays X-ray photoelectron spectra (XPS) of the W 4f, O 1s, and Cu 2p core levels, respectively. In Figure 3(a), W 4f core level spectra of a thick film of $(WO_3)_3$ clusters (~17 monolayers), condensed on the Cu−O surface at 80 K, is compared to the spectrum of the Cu−W−O monolayer. The W $4f_{7/2}$ core level emission peak of condensed $(WO_3)_3$ clusters occurs at a binding energy of 35.9 eV, which is typical for the 6+ oxidation state of the W atoms in the cluster.[21,22] In the Cu−W−O phase, the W $4f_{7/2}$ core level peak is shifted to the lower binding energy of 34.5 eV, and the line shape is significantly modified. The line shape in the tungstate phase is asymmetric with a very narrow width: 0.26 eV at fwhm *versus* 1.05 eV fwhm in the $(WO_3)_3$ cluster film. Overall, the 4f core level spectra convey that the Cu−W−O phase is a very well-defined new surface compound, but further implications may be derived. The 4f line shape of the Cu−W−O layer, in fact one of the narrowest core level line widths measured for an oxide,[23] indicates: (i) there is only one type of W cations in the layer; *i.e.*, all W atoms have the same chemical surrounding and bonding situation; (ii) the oxide layer is well ordered with very few defects; (iii) there is no Franck−Condon vibrational broadening in the photoelectron excitation process;[23] (iv) the asymmetric profile suggests metallic screening in the photoemission final state.[24] The O 1s core level spectrum of Cu−W−O (Figure 3(b)) has an asymmetric tail toward lower binding energy and contains two O 1s spectral components at 529.9 and 530.6 eV binding energy,[25] suggesting that two inequivalent oxygen species are present in the structure (note that the O 1s binding energy of the Cu-(2 × 1)O surface is at 529.7 eV). The Cu 2p XPS spectra (Figure 3(c)) have been recorded in normal emission (NE) and grazing emission (GE) geometry, increasing the surface sensitivity and thus emphasizing surface species in the latter geometry. The fitting of the spectral curves requires two components, which are associated with emission from Cu atoms in the surface region (1) and from the bulk (2). The XPS signal of the Cu bulk component (2) is stronger at normal emission (bottom panel of Figure 3(c)) in accord with the respective higher sensitivity in NE, whereas the surface component is emphasized in grazing emission (top panel). The latter is a clear indication that Cu atoms are involved in the surface layer of the Cu−W−O phase.

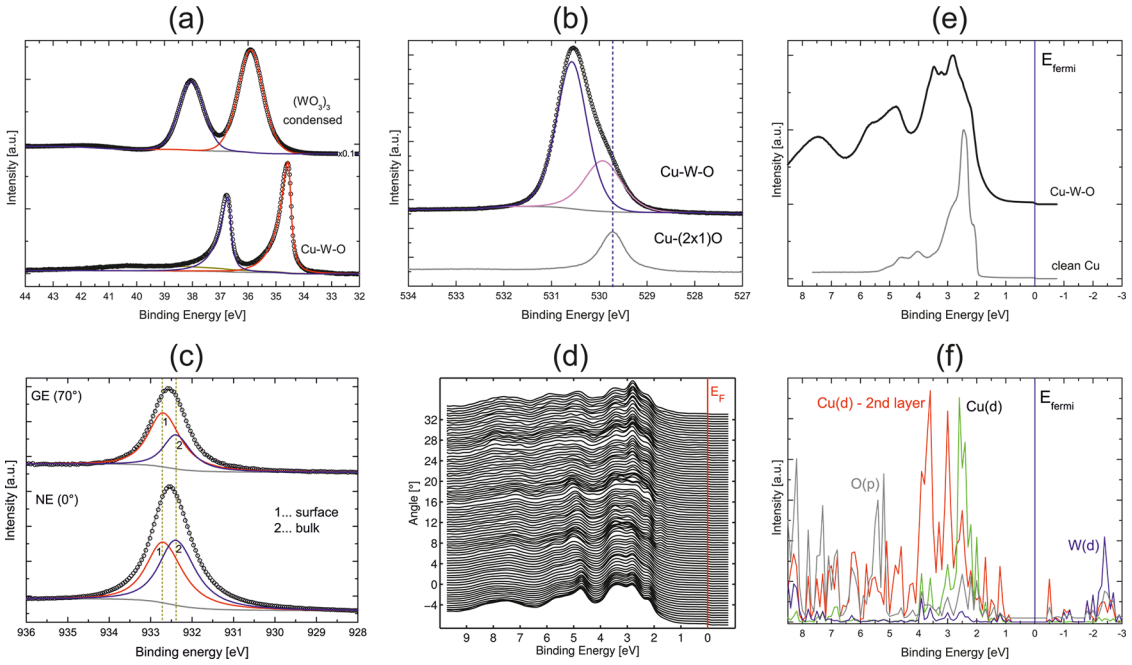

Figure 3. Core level and valence band photoelectron spectroscopy. (a−c) X-ray photoelectron spectra (XPS) of the W 4f, O 1s, and Cu 2p core levels, respectively. The Cu 2p spectra in (c) have been measured at normal emission (NE) and grazing emission (GE) angles. (d) Experimental angle-resolved photoemission difference spectra [$CuWO_4$ − Cu(110)] measured in the [1−10] azimuth, corresponding to the $\bar{\Gamma} - \bar{X}$ substrate surface Brillouin zone direction. The spectra have been recorded at 0.5° intervals from −5.3° to +35.2° with respect to the surface normal (photon energy $h\nu$ = 30 eV). (e) Experimental angle-integrated photoemission spectrum of $CuWO_4$, compared to the clean Cu(110) spectrum at $h\nu$ = 30 eV. (f) Projected density of states (PDOS) onto Cu(3d), O(2p), and W(5d) atomic orbitals. In (d−f) the Fermi energy is at 0 eV.

NEXAFS spectroscopy, which probes the empty electronic states and the chemical environment of the absorbing atom *via* symmetry and crystal field effects, provides a sensitive and characteristic fingerprint of oxide phases.[26] The O K-edge NEXAFS fingerprint of the Cu−W−O is distinctly different from those of the W oxide cluster film or of the Cu(2 × 1)O surface (see Figure S3 in the SI), and this confirms that the Cu−W−O layer is a defined new compound phase.

The complete atomistic structure of the Cu−W−O phase is then derived from first-principles density-functional theory (DFT) simulations (see the SI for technical details). Assuming a (5 × 2) superlattice, a slab periodic model of a Cu(110) surface is set up, several Cu−W−O phases with selected $Cu_xW_yO_z$ composition adsorbed on one side of the slab are considered, and for each of them the structure of the putative global minimum at the given composition is searched for *via* a DFT biased search based on high temperature *ab initio* molecular dynamics followed by geometry optimizations (see the SI for more details).[27] To compare formation energies of different phases, when the stoichiometry can be expressed as a linear combination of N_{WO3} WO_3 and N_{CuO} CuO units, we use the following formula:

$$\Delta E_1 = E_{total} - N_{CuO}E_{CuO} - N_{WO3}E_{WO3} - E_{Cu110} \quad (1)$$

where E_{total} is the total energy of the given configuration, E_{CuO} is the energy needed to remove a CuO pair from the Cu(110)-(2 × 1)O phase, E_{WO3} is one-third of the energy of a $(WO_3)_3$ cluster in the gas phase, and E_{Cu110} is the energy of the Cu(110) slab. For a general $Cu_xO_z(WO_3)_y$ stoichiometry, eq 1 is slightly modified as follows:

$$\Delta E_2 = E_{total} - zE_{O(2\times1)} - xE_{Cu} - yE_{WO3} - E_{Cu110} \quad (2)$$

where $E_{O(2\times1)}$ is the energy needed to remove a CuO pair from the Cu(110)-(2 × 1)O phase, and E_{Cu} is the energy of a bulk Cu atom. Eqs 1 and 2 assume that the WO_3 component comes from deposited W oxide trimers, and oxygen under UHV conditions is provided by the Cu(110)-(2 × 1)O phase, while Cu can either come from the same Cu−O phase or from the bulk of the Cu support (ΔE values do not change qualitatively with either choice). The results of these simulations in the case that the Cu−W−O stoichiometry is a linear combination of N_{WO3} WO_3 and N_{CuO} CuO units are summarized at the bottom of Figure 2(e), in which ΔE_1 values are reported as a function of N_{WO3} and N_{CuO}. From this figure it is apparent that ΔE_1 has a clear minimum at $(N_{WO3}, N_{CuO}) = (4,4)$. That this is a minimum also with respect to oxygen stoichiometry is demonstrated by Figure S4 of the SI, in which ΔE_2 at $y = x = 4$ is plotted as a function of z, and again is found to be minimal at $z = 4$. The global minimum configuration is depicted in Figure 2(e) top and middle panels and corresponds to a monolayer of the $CuWO_4$ ternary

oxide with an atomic arrangement in three sublayers from the surface. In this arrangement, WO_4 tetrahedra rest on the Cu(110) substrate with 2 oxygen atoms interacting directly with Cu, while 2 oxygens on the opposite side of the W-centered tetrahedron reach the topmost level and are interconnected by [1−10] lines of Cu ions. It can be noted that tungsten is tetrahedrally coordinated as in $CaWO_4$ bulk scheelite (a common example of metal tungstate), while the Cu−O−W−O/Cu stacking sequence is vaguely related to $CuWO_4$ bulk wolframite, in which however W has octahedral coordination.[2,19] The Cu atoms in the oxide have two oxygen atoms aligned in a 1-D line and are stabilized at such low coordination by an electron donation from the support, which reduces their positive charge (see below). Such a highly symmetrical configuration, exhibiting only one type of W and Cu cations and two types of O anions, with W buried in the subsurface layer close to the metal support and Cu and half of the O atoms at the topmost level, is perfectly in tune and rationalizes the experimental data discussed above. It should be added in passing that although the global minimum structure appears highly symmetric, a closer inspection reveals that there is a residual mismatch in atomic positions with respect to the underlying Cu(110) support, and a perfect epitaxy can never be reached, thus justifying the incommensurate character of the phase. This combination of robustness and geometrical frustration endows the system with a great, yet precisely localized, structural flexibility (see the floppy vibrational modes discussed in the next paragraph and the existence of closely lying isomeric structures reported in the SI), and may be a common feature of ternary oxide-on-metal systems.

To complete comparison with experiment, we have also calculated the XPS binding energies of the various atoms and found 35.5 ± 0.1, 539.15 ± 0.15, 538.8 ± 0.2, 938.7 ± 0.1, and 938.1 ± 0.1 eV, for W 4f, O 1s top layer, O 1s interface layer, Cu 2p top layer, and Cu 2p interface layer core levels, respectively. Note that we use a scalar relativistic Hamiltonian, so that the predicted value for W should be compared with an average of $4f_{7/2}$ and $4f_{5/2}$ experimental peaks (see the SI for technical details) and that the reported uncertainties relate to the scattering of values on the differently located atoms. The W XPS core level binding energy is in quantitative agreement with experimental data in Figure 3, while for O and Cu our theoretical approach is less precise in absolute value but is able to correctly predict the ordering between topmost and buried atoms, further confirming the proposed structural assignment.

The peculiar structure of 2-D $CuWO_4$ presents uncommon phonon properties and features. In bulk WO_3 W−O−W vibrational stretching modes give rise to characteristic bands at 711 and 806 cm^{-1}, whereas a phonon peak at higher frequency (987 cm^{-1}) only

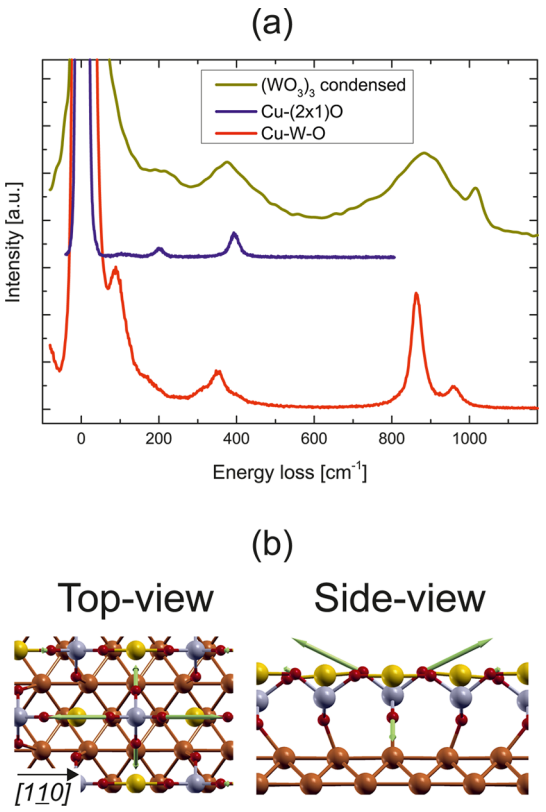

Figure 4. Phonons. (a) High-resolution electron energy loss spectrum (HREELS) of the 2-D $CuWO_4$ system (Cu−W−O, in red), compared to the Cu-(2 × 1)O bare substrate (in blue) and to a thick film of $(WO_3)_3$ clusters (in green). (b) Top and side views of the high-frequency vibrational mode at 935 cm^{-1} as predicted at the DFT level. The green arrows indicate the direction of atomic displacements.

appears after partial breaking of the W−O−W bonding network due to doping and corresponding formation of W═O tungstyl groups,[28] so that vibrational absorption above 950 cm^{-1} is usually assumed to be experimental proof of the presence of tungstyls. The $CuWO_4$ 2-D phase does indeed present a strong band at 960 cm^{-1} in the high-resolution electron energy loss spectrum (HREELS) (see Figure 4(a)), but contrary to usual expectations this is explained by DFT phonon simulations as a W−O stretching of the WO_4 tetrahedra rather than as tungstyl vibrational modes, as depicted in Figure 4(b) (the DFT-predicted frequency is 935 cm^{-1} and is the highest one in the system). Another peculiar feature of the 2-D $CuWO_4$ phase singled out by DFT calculations is the presence of vibrational modes at very low frequencies (below 30 cm^{-1}, too low to be detected in the HREELS spectrum), the lowest of which mostly consists of oscillations along the [001] direction and involves one row of Cu, W, and O atoms every four in the unit cell; see Figure 5(b). This strongly anisotropic soft mode has visible consequences in STM images. From Figure 2(b), it can be seen that the experimental STM bright maxima are elongated along the [001] direction and nearly merge into a continuous line roughly one every four rows, which is interpreted in

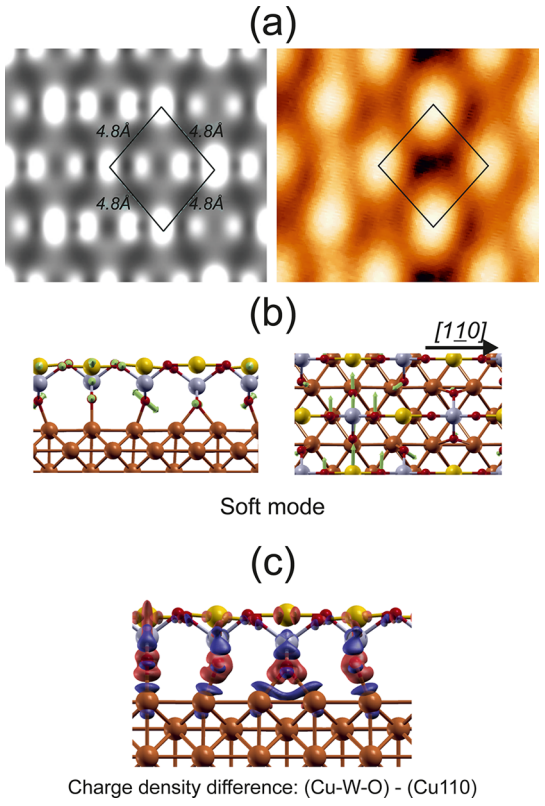

Figure 5. STM and charge distribution. (a) Close-up of an experimental STM image at 1 V bias (right) and the corresponding simulated image (left). (b) Top and side views of the low-frequency (soft) vibrational mode (at <30 cm^{-1}) as predicted at the DFT level (green arrows indicate the direction of atomic displacements). (c) Plot of the difference in electron density between the 2-D $CuWO_4$ phase and its constituting fragments (red: charge density increase, blue: charge density depletion).

the light of the DFT phonon analysis as due to the zero-point motions connected with the lowest-frequency mode. Figure 5(a) reports a close-up of an experimental STM image at 1 V bias (right) and the corresponding simulated image (left). We are unable to introduce the vibrational broadening effect into our STM simulations, which thus show only well-separated bright protrusions: topmost Cu atoms are predicted to be mostly visible, although side maxima are also present due to topmost oxygens. Considering the limitation due to neglecting zero-point motions, we find a reasonable comparison between experimental and simulated STM images in Figure 5(a); see the SI for a more detailed discussion.

A fair agreement is also found between the experimentally measured and predicted values of the 2-D $CuWO_4$ work function, of 5.2 $\pm$ 0.1 and 5.05 eV, respectively. Note that a similar agreement between experiment and theory is also found for the precursor systems: Cu(110), whose work function values are 4.6 (experiment) and 4.4 eV (prediction), respectively, and the Cu(110)-(2 $\times$ 1)O surface oxide phase, whose values are 5.1 and 4.7 eV, respectively. The work function is a basic electronic quantity, important among other things because it is connected to the charge transfer between the Cu(110) support and the 2-D $CuWO_4$ phase. The reasonable agreement between theory and experiment makes us confident in a more detailed analysis of the system electron density. A plot of the electron density difference between the 2-D $CuWO_4$ phase and its constituting fragments, an isolated $CuWO_4$ monolayer and the Cu(110) support (both geometries frozen in the interacting configuration), is shown in Figure 5(c), from which it is apparent that Cu transfers a significant amount of charge (about 2−3 electrons per unit cell from a Bader analysis, see the SI) to the $CuWO_4$ phase. Both Cu and W atoms receive this charge donation, reducing their oxidation state by ~0.5 elementary charge unit with respect to bulk $CuWO_4$ (the Bader charges read ~0.7 and ~2.9 for Cu and W, respectively), while the O atoms result somewhat less negative with respect to the bulk phase. It should be noted parenthetically that the XPS core level shifts do not simply correlate with charge state of the corresponding atom.

To further deepen the analysis of the system electronic structure, we plot in Figure 3(f) the projected density of states (PDOS) onto Cu(3d), O(2p), and W(5d) atomic orbitals and compare it to experimental angle-resolved and angle-integrated photoemission spectra: Figure 3(d,e), respectively. Note that the angle-resolved photoemission spectra in Figure 3(d) are difference spectra [$CuWO_4$ minus clean Cu(110)]; see the SI for further details. A good agreement between theory and experiment is again observed. The non-dispersive peak at ~2 eV below the Fermi energy can be put in correspondence with the nonbonding Cu 3d peak of the surface layer in the PDOS, while the weakly dispersive structures at 4.5−8 eV below the Fermi energy may be associated with oxygen 2p bonding states, hybridized with W and Cu states. The flat band at ~3−4 eV is presumably related to the Cu 3d states in the second layer at the interface; see the high DOS feature at that energy in Figure 3(f). A band gap of ~1.2 eV is predicted by theory, and low-energy excitations correspond to promoting electrons from interfacial Cu atoms into W 5d and O 2p states, as well as interfacial Cu ones, being thus different from those of bulk $CuWO_4$,[7] while at excitation energies of about 2 eV O-to-W transitions should also arise. The most striking feature of the angle-integrated photoemission spectrum is a significant intensity over a much broader interval of binding energies with respect to the Cu(110) surface: this, combined with the small band gap, makes this phase promising in terms of photoelectrocatalytic properties.[8]

CONCLUSION

In summary, the preparation here reported of well-ordered 2-D ternary Cu−W oxide material *via* a

controlled solid state reaction using a binary surface oxide and molecular oxide clusters from the gas phase represents an unconventional fabrication route that exploits the atomic scale precision capabilities of ultra-high vacuum surface science methodology, and it can be easily generalized to a wide class of oxide materials. The resulting stoichiometric, near-defect-free 2-D $CuWO_4$ oxide is an ideal model laboratory for understanding structure−property relationships in complex low-dimensional oxide systems as it allows a synergistic experimental and theoretical unprecedented level of characterization. It turns out that the present 2-D $CuWO_4$ phase exhibits peculiar electronic and vibrational properties, combining a robust framework with localized regions of flexibility in structure and stoichiometry, and displaying a reduced band gap and increased density of states close to the Fermi level with respect to the bulk. Although its chemical properties are yet to be explored and will be the subject of future investigations, these unique features enroll it with promising perspectives into the class of novel monolayer catalysts, consisting of a 2-D oxide material in combination with a suitable substrate that have been shown to possess great potential for nanocatalysis,[29−31] with the additional benefit in the present case of possible coupling with significant optical response in the visible region.

METHODS

The experiments have been performed in several UHV systems, all with base pressures $\leq 1 \times 10^{-10}$ mbar. STM measurements were carried out in a low-temperature (5 K) STM system (Createc, Germany) using electrochemically etched W tips in a constant current mode. Vibrational surface spectra were measured with high-resolution electron energy loss spectroscopy in a custom-designed Delta 0.5 HREELS spectrometer (SPECS, Germany). Photoemission spectra and X-ray absorption spectra were obtained with use of synchrotron radiation at beamline I311 in the Swedish synchrotron radiation laboratory Maxlab (XPS) and at the APE beamline at the Italian Sincrotrone Trieste ELETTRA (angle- integrated and angle-resolved valence band photoemission). All UHV systems were equipped with LEED optics facilities, which provided the link between the surface preparations in the different systems and ensured the same surface phases *in situ* prepared being measured. The Cu(110)-(2×1)O surface reconstruction has been prepared by exposing the clean Cu(110) surface to 15L (1 Langmuir (L) = 1×10^{-6} Torr sec) O_2 at 600 K. The $(WO_3)_3$ cluster beam was generated by thermal sublimation of WO_3 powder at 1300 K in a thermal evaporator; the evaporation flux was monitored by quartz microbalance.

Density-functional calculations were performed using the plane-wave Quantum Espresso (QE) package[32] and the Perdew-Burke-Ernzerhof (PBE) exchange-correlation functional.[33] *Ab initio* molecular dynamics (AIMD) simulations were performed in a (5×2) rectangular cell of a Cu(110) slab with one $Cu_xW_yO_z$ layer at the top varying the (x,y,z) composition and the initial configuration. A structural search for the optimal system stoichiometry is performed as described in the SI. STM images, charge analysis, and core−electron shifts are evaluated using the same DFT approach and QE code. Full technical details are provided in the SI.

Conflict of Interest: The authors declare no competing financial interest.

Acknowledgment. This scientific program has been supported by the ERC Advanced Grant SEPON.

Supporting Information Available: Structure of the Cu−W−O layer; electronic band mapping by angle-resolved UV photoelectron spectroscopy (ARUPS); near-edge X-ray absorption fine structure (NEXAFS); theory−technical details. This material is available free of charge *via* the Internet at http://pubs.acs.org.

REFERENCES AND NOTES

1. Kuzmin, A.; Purans, J.; Kalendarev, R.; Pailharey, D.; Mathey, Y. XAS, XRD, AFM and Raman Studies of Nickel Tungstate Electrochromic Thin Films. *Electrochim. Acta* **2001**, *46*, 2233–2236.
2. Kuzmin, A.; Purans, J. Local Atomic and Electronic Structure of Tungsten Ions in AWO_4 Crystals of Scheelite and Wolframite Types. *Radiat. Meas.* **2001**, *33*, 583–586.
3. Fujita, M.; Itoh, M.; Katagiri, T.; Iri, D.; Kitaura, M.; Mikhailik, V. B. Optical Anisotropy and Electronic Structures of $CdMoO_4$ and $CdWO_4$ Crystals: Polarized Reflection Measurements, X-ray Photoelectron Spectroscopy, and Electronic Structure Calculations. *Phys. Rev. B: Condens. Matter Mater. Phys.* **2008**, *77*, 155118.
4. Ruiz-Fuertes, J.; Sanz-Ortiz, M. N.; González, J.; Rodríguez, F.; Segura, A.; Errandonea, D. Optical Absorption and Raman Spectroscopy of $CuWO_4$. *J. Phys.: Conf. Ser.* **2010**, *215*, 012048.
5. Atuchin, V. V.; Troitskaia, I. B.; Khyzhum, O. Yu.; Bekenev, V. L.; Solonin, Yu. M. Electronic Properties of h-WO_3 and $CuWO_4$ Nanocrystals as Determined from X-ray Spectroscopy and First-Principles Band-Structure Calculations. *Int. J. Appl. Phys. Math.* **2011**, *1*, 19–23.
6. Lalic, M. V.; Popovic, Z. S.; Vukajlovic, F. R. *Ab Initio* Study of Electronic, Magnetic and Optical Properties of $CuWO_4$ Tungstate. *Comput. Mater. Sci.* **2011**, *50*, 1179–1186.
7. Lalic, M. V.; Popovic, Z. S.; Vukajlovic, F. R. Electronic Structure and Optical Properties of $CuWO_4$: An *Ab Initio* Study. *Comput. Mater. Sci.* **2012**, *63*, 163–167.
8. Jourey, J. E.; Bartlett, B. M. Electrochemical Deposition and Photoelectrochemistry of $CuWO_4$, a Promising Photoanode for Water Oxidation. *J. Mater. Chem.* **2011**, *21*, 7651–7660.
9. Chang, Y.; Braun, A.; Deangekis, A.; Kaneshiro, J.; Gaillard, N. Effect of Thermal Treatment on the Crystallographic, Surface Energetics, and Photoelectrochemical Properties of Reactively Cosputtered Copper Tungstate for Water Splitting. *J. Phys. Chem. C* **2011**, *115*, 25490–25495.
10. Jourey, J. E.; Kurtz, J. B.; Bartlett, B. M. Water Oxidation on a $CuWO_4$-WO_3 Composite Electrode in the Presence of $[Fe(CN)_6]^{3-}$: Toward Solar Z-Scheme Water Splitting at Zero Bias. *J. Phys. Chem. C* **2012**, *116*, 3200–3205.
11. Janaky, C.; Rajeshwar, K.; de Tacconi, N. R.; Chanmanee, W.; Huda, M. N. Tungsten-Based Oxide Semiconductors for Solar Hydrogen Generation. *Catal. Today* **2013**, *199*, 53–64.
12. Heyer, O.; Hollmann, N.; Klassen, I.; Jodlauk, S.; Bohaty, L.; Becker, P.; Mydosh, J. A.; Lorenz, T.; Khomskii, D. A New Multiferroic Material: $MnWO_4$. *J. Phys.: Cond. Matter* **2006**, *18*, L471–L475.
13. Taniguchi, K.; Sato, M.; Arima, T. Optical Imaging of Coexisting Collinear and Spiral Spin Phases in the Magnetoelectric Multiferroic $MnWO_4$. *Phys. Rev. B: Condens. Matter Mater. Phys.* **2010**, *81*, 0664406.
14. Surnev, S.; Fortunelli, A.; Netzer, F. P. Structure-Property Relationship and Chemical Aspects of Oxide-Metal Hybrid Nanostructures. *Chem. Rev.* **2013**, *113*, 4314–4372.
15. Pomp, S. Interaction of $(WO_3)_3$ Clusters with Bare Ni(110) and Oxygen Reconstructed O-Ni(110) Surfaces. Master Thesis, Karl-Franzens-University of Graz, Graz, Austria, September 2013.

16. Dürr, H.; Fauster, Th.; Schneider, R. Surface Structure Determination of the (2 × 1)O-Cu(110) Reconstruction by Low-Energy Ion Scattering. *Surf. Sci.* **1991**, *244*, 237–246.
17. Maleknia, S.; Brodbelt, J.; Pope, K. Characterization of the Reactive and Dissociative Behavior of Transition Metal Oxide Cluster Ions in the Gas Phase. *J. Am. Soc. Mass Spectrom.* **1991**, *2*, 212–219.
18. Wagner, M.; Surnev, S.; Ramsey, M. G.; Barcaro, G.; Sementa, L.; Negreiros, F. R.; Fortunelli, A.; Dohnalek, Z.; Netzer, F. P. Structure and Bonding of Tungsten Oxide Clusters on Nanostructured Cu-O Surfaces. *J. Phys. Chem. C* **2011**, *115*, 23480–23487.
19. Kihlborg, L.; Gebert, E. $CuWO_4$, a Distorted Wolframite-Type Structure. *Acta Crystallogr., Sect. B: Struct. Crystallogr. Cryst. Chem.* **1970**, *26*, 1020–1026.
20. Lang, N. D. Theory of Single-Atom Imaging in the Scanning Tunneling Microscope. *Phys. Rev. Lett.* **1986**, *56*, 1164–1167.
21. Katrib, A.; Hemming, F.; Wehrer, P.; Hilaire, L.; Maire, G. The Multi-Surface Structure and Catalytic Properties of Partially Reduced WO_3, WO_2 and WC + O_2 or W + O_2 as Characterized by XPS. *J. Electron Spectrosc. Relat. Phenom.* **1995**, *76*, 195–200.
22. Li, Z.; Zhang, Z.; Kim, Y. K.; Smith, R. S.; Netzer, F.; Kay, B. D.; Rousseau, R.; Dohnalek, Z. Growth of Ordered Ultrathin Tungsten Oxide Films on Pt(111). *J. Phys. Chem. C* **2011**, *115*, 5773–5783.
23. Nelin, C. J.; Bagus, P. S.; Brown, M. A.; Sterrer, M.; Freund, H.-J. Analysis of the Broadening of X-ray Photoelectron Spectroscopy Peaks for Ionic Crystals. *Angew. Chem., Int. Ed.* **2011**, *50*, 10174–10177.
24. Doniach, S.; Sunjic, M. Many-Electron Singularity in X-ray Photoemission and X-ray Line Spectra from Metals. *J. Phys. C: Solid State Phys.* **1970**, *3*, 285–291.
25. The XPS core level spectra have been fitted using a commercial least-squares minimization software: Fairley, N. *CasaXPS*, Version 2.3.15; Casa Software, Ltd.: Teignmouth, U.K., 2009.
26. de Groot, F. High-Resolution X-ray Emission and X-ray Absorption Spectroscopy. *Chem. Rev.* **2011**, *101*, 1779–1808.
27. Barcaro, G.; Aprà, E.; Fortunelli, A. Structure of Ag Clusters Grown on F_S-Defect Sites of an MgO(100) Surface. *Chem.—Eur. J.* **2007**, *13*, 6408–6418.
28. Manciu, F. S.; Yun, Y.; Durrer, W. G.; Howard, J.; Schmidt, U.; Ramana, C. V. Comparative Microscopic and Spectroscopic Analysis of Temperature-Dependent Growth of WO_3 and $W_{0.95}Ti_{0.05}O_3$ Thin Films. *J. Mater. Sci.* **2012**, *47*, 6593–6600.
29. Sim, U.; Yang, T.; Moon, J.; An, J.; Hwang, J.; Seo, J. H.; Lee, J.; Kim, K. Y.; Lee, J.; Han, S.; *et al.* N-Doped Monolayer Graphene Catalyst on Silicon Photocathode for Hydrogen Production. *Energy Environ. Sci.* **2013**, *6*, 3658–3664.
30. Abdul Wasey, A. H. M.; Chakrabarty, S.; Das, G. P.; Majumder, C. h-BN Monolayer on the Ni(111) Surface: a Potential Catalyst for Oxidation. *ACS Appl. Mater. Interfaces* **2013**, *5*, 10404–10408.
31. Fu, Q.; Yang, F.; Bao, X. H. Interface-Confined Oxide Nanostructures for Catalytic Oxidation Reactions. *Acc. Chem. Res.* **2013**, *46*, 1692–1701.
32. Giannozzi, P.; Baroni, S.; Bonini, N.; Calandra, M.; Car, R.; Cavazzoni, C.; Ceresoli, D.; Chiarotti, G. L.; Cococcioni, M.; Dabo, I.; *et al.* QUANTUM ESPRESSO: a Modular and Open-Source Software Project for Quantum Simulations of Materials. *J. Phys.: Condens. Matter* **2009**, *21*, 395502.
33. Perdew, J.; Burke, K.; Ernzerhof, M. Generalized Gradient Approximation Made Simple. *Phys. Rev. Lett.* **1996**, *77*, 3865–3868.